THE JOURNAL OF PHYSICAL CHEMISTRY B

Article

pubs.acs.org/JPCB

Segmental Relaxations and Crystallization-Induced Phase Separation in PVDF/PMMA Blends in the Presence of Surface-Functionalized Multiwall Carbon Nanotubes

Maya Sharma,[†] Keshav Sharma,[†] and Suryasarathi Bose*

Department of Materials Engineering, Indian Institute of Science, Bangalore-560012, India

ABSTRACT: Crystallization-induced phase separation and segmental relaxations in poly(vinylidene fluoride)/poly(methyl methacrylate) (PVDF/PMMA) blends was systematically investigated by melt-rheology and broadband dielectric spectroscopy in the presence of multiwall carbon nanotubes (MWNTs). Different functionalized MWNTs (amine, $-NH_2$; acid, $-COOH$) were incorporated in the blends by melt-mixing above the melting temperature of PVDF, where the blends are miscible, and the crystallization induced phase separation was probed in situ by shear rheology. Interestingly, only $-NH_2$ functionalized MWNTs (a-MWNTs) aided in the formation of β-phase (*trans*−*trans*) crystals in PVDF, whereas both the neat blends and the blends with $-COOH$ functionalized MWNTs (c-MWNTs) showed only α-phase (*trans*−*gauche*−*trans*−*gauche*′) crystals as inferred from wide-angle X-ray diffraction (WXRD) and Fourier transform infrared (FTIR). Furthermore, blends with only a-MWNTs facilitated in heterogeneous nucleation in the blends manifesting in an increase in the calorimetric crystallization temperature and hence, augmented the rheologically determined crystallization induced phase separation temperature. The dielectric relaxations associated with the crystalline phase of PVDF (α_c) was completely absent in the blends with a-MWNTs in contrast to neat blends and the blends with c-MWNTs in the dielectric loss spectra. The relaxations in the blends investigated here appeared to follow Havriliak−Negami (HN) empirical equations, and, more interestingly, the dynamic heterogeneity in the system could be mapped by an extra relaxation at higher frequency at the crystallization-induced phase separation temperature. The mean relaxation time (τ_{HN}) was evaluated and observed to be delayed in the presence of MWNTs in the blends, more prominently in the case of blends with a-MWNTs. The latter also showed a significant increase in the dielectric relaxation strength ($\Delta\varepsilon$). Electron microscopy and selective etching was used to confirm the localization of MWNTs in the amorphous phases of the interspherulitic regions as observed from scanning electron microscopy (SEM). The evolved crystalline morphology, during crystallization-induced phase separation, was observed to have a strong influence on the charge transport processes in the blends. These observations were further supported by the specific interactions (like dipole induced dipole interaction) between a-MWNTs and PVDF, as inferred from FTIR, and the differences in the crystalline morphology as observed from WXRD and polarized optical microscopy (POM).

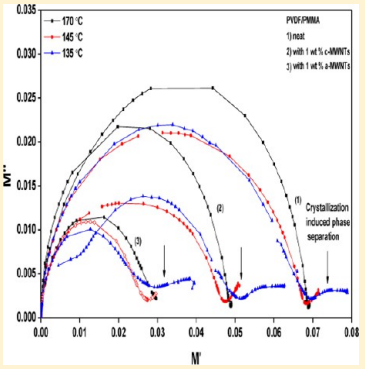

INTRODUCTION

It is generally agreed upon that blends of poly(vinylidene fluoride) (PVDF) and poly(methyl methacrylate) (PMMA) are completely miscible, at all compositions, in the melt state due to strong intermolecular interactions arising from hydrogen bonding between carbonyl groups in PMMA and $-CH_2$ groups of PVDF and the dipole−dipole interactions between $-CH_2$ of PMMA and CF_2 in PVDF. Blends of PVDF/PMMA exhibit lower critical solution temperature (LCST) at temperatures >330 °C.[1,2] Interestingly, on cooling from the melt, they show upper critical solution temperature (UCST) strongly dependent on the blend composition, and the rate of cooling and was first reported by Inoue et al.[3] Both liquid−liquid and crystallization-induced phase separation is believed to be the underlying mechanisms of phase separation in PVDF/PMMA blends. It has also been envisaged that both crystallization and liquid−liquid phase separation occur, often competing with each other.[4] Using light scattering, Saito et al.[5] could resolve the competitive process of crystallization-induced and liquid−liquid phase separation in blends of PVDF/PMMA and suggested that the latter precedes the former. Below the calorimetric crystalline melting temperature (T_m), PVDF crystallizes from the melt, especially with high PVDF concentration (PVDF ≥ 50%) in the blends.[6,7] On the basis of the rate of cooling from the melt, different crystalline morphology has been identified in PVDF: a crystalline region, an liquid-like amorphous region, and a crystalline−amorphous interphase.[8] For the blends with PVDF< 40%, no crystallization takes place either upon slow cooling from the melt or by annealing at a temperature above its glass transition temperature (T_g).[9]

Phase separation in polymer blends can be probed using different techniques like light scattering, optical microscopy, solid state NMR, electron microscopy, and so on.[5,10−12] However, multiple scattering becomes dominant in complex

Received: April 5, 2013
Revised: May 23, 2013
Published: June 24, 2013

   dx.doi.org/10.1021/jp4033723 | J. Phys. Chem. B 2013, 117, 8589−8602

systems like blends with nanoparticles (NPs) and limits the use of optical/scattering techniques. In this context, rheology can shed more light on the transition temperatures, provided the spatial resolution of the evolving phases are large enough to contribute to the elastic stresses.[13] Rheological fingerprints are very sensitive to the changes in the viscoelastic properties in homogeneous as well as in the two phase regime of partially miscible polymer blends. This can be realized as in the case of blends with weak dynamically asymmetry where the rheological signals are frail,[14] which otherwise results in a prominent upturn in the elastic modulus, particularly in the vicinity of phase transition temperature, for strong dynamically asymmetric blends.[15] In the case of weak dynamically asymmetric blends, matching segmental dynamics (due to small difference in T_g) makes the rheological material function almost insensitive to detect any changes in viscoelastic properties of the blend in the vicinity of phase separation. On the other hand, in the blends with strong dynamic asymmetry (large difference in T_g) a fair difference between segmental dynamics of the constituents and large concentration fluctuation make rheology an important tool to detect phase separation temperature.

In the recent past, it was realized that the NPs can also compatibilize binary blends besides offering intriguing functional properties. However, the mechanism of stabilization was different from the classical compatibilization rendered by block copolymers. Lipatov et al.[16] reported that the addition of NPs changes the interaction parameter between the components in the blends and hence the phase separation temperature. Recently, Ginzburg proposed a simple model that explicates the effect of particle volume fraction on the miscibility of polymer blends.[17] However, the existing models can only predict the phase separation temperature of the blends with spherical NPs, and further research is needed to understand the effect of size and shapes of the NPs on the dynamics and kinetics of phase separation. Notably, the effect of carbon nanotubes (CNTs) which are rather flexible, coiled, rod-like particles needs more understanding on the phase separation mechanism. The highly curved surface of CNTs makes adsorption of macromolecules difficult and often decreases the effective surface concentration of the adsorbed entity.[18] However, their exceptional properties, which are a direct consequence of high aspect ratio and high specific surface area, makes CNTs interesting candidates in the field of polymer-based nanocomposites and has attracted a great deal of interest in the recent past (for a recent review, see ref 19). More specifically, CNT-based polymer composites have received lot of attention in the recent past, as CNTs dramatically increase the permittivity as well as electrical conductivity of composites at very low concentrations.[20−22] Apart from electrical conductivity, inclusion of CNTs and other carbon nanomaterials in PVDF can also induce piezoelectric behavior by forming β-phase.[23] Recently, Hou et al.[24] reported alkyl-functionalized graphene/poly(dimethyl silicone) nanocomposites, which show promising piezoresistivity property.

CNTs act as a heteronucleating agent often manifesting in an upshift in the calorimetric crystallization temperature (T_c), although the effect strongly depends on the matrix polymer. Recent papers highlight the unusual crystallization, especially with polar polymers in the presence of CNTs due to various molecular-level conformations.[25] These observations were related with the confinement effect and/or improved interfacial adhesion with the polar polymers. These effects could be of interest in particular for blends of PVDF/PMMA, where in the distinct morphological components like the crystalline region, the liquid-like interzonal region and the interphase can strongly be influenced in the presence of heterogeneity and more specifically on the nature of interactions with the matrix host. The associated changes can be mapped by probing, in situ, the evolution of interfaces, interface-driven elasticity, and the segmental chain dynamics using various spectroscopy (mechanical and dielectric). In this paper we present a comprehensive view of segmental relaxations and crystallization-induced phase separation in PVDF/PMMA blends in the presence of different functionalized MWNTs. This was accomplished by performing rheology and dielectric spectroscopy, *in situ*, in the frequency domain for a particular blend (70/30 wt/wt, PVDF/PMMA) and at a particular concentration of MWNTs (1 wt %) at different temperatures. The crystalline morphology was studied by polarized optical microscopy (POM) and wide-angle X-ray diffraction (WXRD). The annealed and phase-separated morphologies and the positioning of MWNTs in the blends was evaluated using scanning electron microscopy (SEM).

EXPERIMENTAL SECTION

Materials. Both atactic PMMA (Atuglass V825T, with M_w of 95,000 g/mol and polydispersity of 2.1) and PVDF (Kynar-761, with M_w of 44000 g/mol) was kindly provided by Arkema. Carbon vapor deposition-synthesized functionalized multiwall carbon nanotubes (MWNTs) were obtained from Nanocyl CA Belgium. Two types of MWNTs were utilized in this study: amine functionalized (a-MWNTs with average diameter: 9−10 nm; average length: 600−700 nm, $-NH_2$ conc. < 0.4 wt %) and acid functionalized (c-MWNTs with average diameter: 10 nm; average length: 1−1.5 μm, −COOH conc. ∼ 4 wt %). Solvents (glacial acetic acid and acetone) of analytical grade were obtained commercially and were used without further purification.

Blend Preparation. 70/30 (w/w) blends of PVDF/PMMA were prepared with or without 1 wt % MWNTs by melt mixing using a Minilab II HAAKE extruder CTW5 (7 cm^3) at 220 °C with a rotational speed of 60 rpm for 20 min. The extruded blend samples were optically transparent further manifesting the miscibility in the neat blends. The mixing was performed under N_2 atmosphere to prevent oxidative degradation. Samples were predried at 80 °C in a vacuum oven for at least 24 h prior to processing. Melt mixed samples were subsequently compression-molded into discs using a lab scale hydraulic press and were air-cooled to induce crystallization of PVDF.

Characterization. Fourier transform infrared (FTIR) spectra were recorded on a Perkin-Elmer spectrometer GX for thin films using KBr pellets by accumulating 32 scans with a resolution of 4 cm^{-1} over the range 400−4000 cm^{-1}. The possible interactions between MWNTs and the phases are shown in Figure 1. The characteristic peaks at 2992, 2954, 1740, and 1484 cm^{-1} represent CH_2 stretching, C−O−CH_3 stretching, C═O stretching, and CH_2 scissoring of PMMA, respectively. Characteristic peaks at 1409, 1274.8, and 1071 cm^{-1} represent deformed vibration of the CH_2 group of PVDF, symmetric stretching of the CF_2 group, and the CF_2 stretching mode, respectively. Peaks at 977, 874.5, 854, 798, 763, 614.3, and 530.6 cm^{-1} represent the α phase (*trans*−*gauche*−*trans*−*gauche*′) structure of PVDF. It is clear from Figure 1a that the stretching of the CF_2 group in a-MWNTs at 1139 and 1065 cm^{-1} shift significantly to a higher wavenumber with respect to

dx.doi.org/10.1021/jp4033723 | J. Phys. Chem. B 2013, 117, 8589−8602

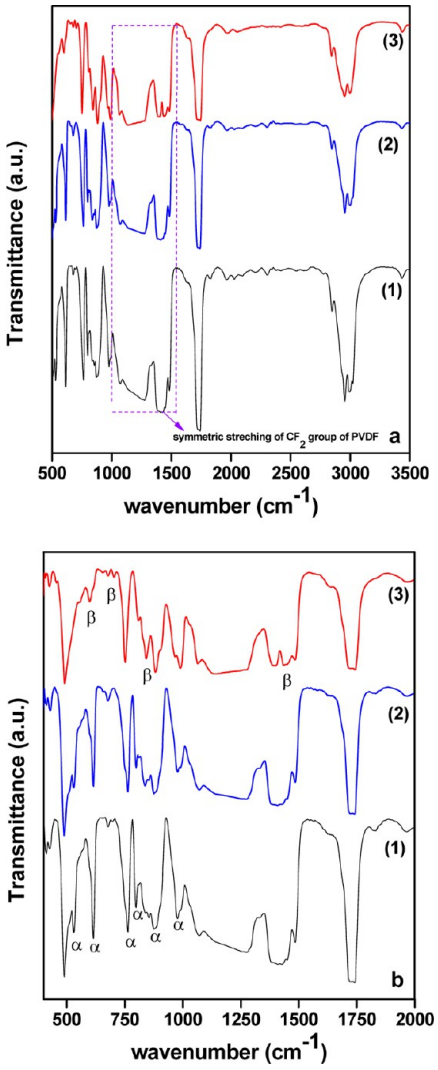

Figure 1. (a) FTIR spectra for neat 70/30 PVDF/PMMA blends and blends with MWNTs. (b) Magnified view of the FTIR spectra in the region 400−2000 cm^{-1} (sub parts 1−3 indicate the spectra for neat blends and for blends with 1% c-MWNT and 1% a-MWNT, respectively).

the neat blends. This shift in CF_2 stretching and C−F stretching in contrast to neat blends is assigned to dipole−induced-dipole interaction between the $-NH_2$ group of a-MWNTs and the $-CF_2$ group of PVDF. Dipoles induced by $-NH_2$ groups of a-MWNTs further induces the conversion of α-phase (*trans−gauche−trans−gauche'*) crystals into β-phase (*trans−trans*) crystals. The magnified spectra in the range 400−2000 cm^{-1} is shown in Figure 1b. Peaks at 977, 874.5, 853.8, 797.8, 763, 614, and 530 correspond to the α-phase (*trans−gauche−trans−gauche'*) crystals of neat PVDF, which can also be seen in the blends with c-MWNTs; however, only β phase (*trans−trans*) is present in the blends with a-MWNTs manifesting in peaks at 1436, 842.6, 678, and 600 cm^{-1} in the FTIR spectra.[26]

WXRD patterns using a PANalytical X'pert pro was used to study the crystallization and phase behavior of PVDF/PMMA blends in the presence of MWNTs. The scans were obtained using Cu K_α radiation with a wavelength of 1.54 Å and an energy value of 40 k eV. Measurements were taken between 2θ values of 5−50°, with a scan rate of 0.04° sec^{-1}. Figure 2 shows

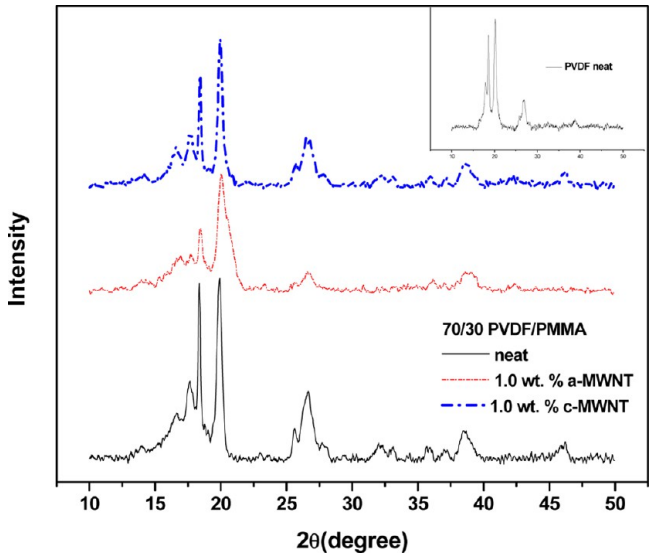

Figure 2. WXRD patterns for neat PVDF/PMMA blends and blends with MWNTs (Inset shows the WXRD patterns for the neat PVDF).

the WAXD pattern for PVDF (inset) and blends of PVDF/PMMA with MWNTs. PVDF exists in four crystalline phases, among which α and β phases are the more common forms. The α-phase crystals are usually produced during melt crystallization under atmospheric pressure and are the most stable form at room temperature.[27] Pure PVDF as well as blends of 70/30 (w/w) PVDF/PMMA indicate the characteristic peaks at 2θ values of 17.6°, 18.35°, 19.88°, and 26.5° corresponding to $\alpha(100)$, $\alpha(020)$, $\alpha(110)$, and $\alpha(021)$ planes, respectively.[28,29] With the addition of a-MWNTs in 70/30 (wt/wt) blend, there is a remarkable decrease in the peak intensity for α phase at 2θ values of 17.6° and 26.5°. Furthermore, the prominent peak at 2θ of 19.9° broadens and shifts to higher 2θ, suggesting the formation of new crystalline phases. This can be assigned to the (110) and (200) reflections of the β-crystal phase. and can be associated with the spatially confined state of PVDF[30] in the presence of MWNTs. However, no change is observed in the position of the peaks in the case of blends with c-MWNTs. Broadening of the peak also indicates that addition of a-MWNTs results in a broader distribution of spherulites as well as decrease in size (by assessing the fwhm of the peaks). The growth of spherulites is hindered as a greater number of crystal nuclei start to impinge on each other in a confined space.[31]

Thermal transitions like glass transition (T_g), melting temperature (T_m), and crystallization temperature (T_c) were determined using differential scanning calorimetry (DSC; Mettler Toledo DSC-1). Prior to measurements, all samples were dried at 80 °C in a vacuum oven for at least 24 h. Samples of about 5−10 mg were cut from the extruded samples and crimped in standard aluminum DSC pans. The temperature scale was calibrated with an indium standard, which has a melting temperature of 156.68 °C and a heat of fusion of 28.45 J/g, prior to the experiments. During first heating cycle, samples were heated at the rate of 10 °C/min over the temperature range of 0−220 °C and subsequently quenched to −50 °C to prevent phase separation. Second heating was performed at the heating rate of 10 °C/min up to 220 °C and slowly cooled to room temperature at 2 °C/min to monitor the crystallization process of PVDF.

dx.doi.org/10.1021/jp4033723 | J. Phys. Chem. B 2013, 117, 8589−8602

Viscoelastic properties of the blends were studied using a stress-controlled Discovery Hybrid Rheometer (DHR-3, TA Instruments) with parallel plate geometry (25 mm in diameter and 1 mm gap distance). Isochronal dynamic temperature ramp measurements were performed at a uniform cooling rate of 0.5 K/min from the single phase (200 °C) to the phase separated regime (120 °C) to detect the onset of phase separation in the blends. A fixed frequency (0.1 rad/s), which is low enough to lie in the terminal regime, was applied, and the strain amplitude was verified to be within the linear viscoelastic region. All measurements were carried out under N_2 atmosphere to prevent any adsorption of moisture or any degradation of sample at high temperature. All experiments were done using axial force control. During these tests, the axial force was compensated to take into account the volumetric changes occurring due to crystallization processes during cooling.

The onset of crystallization and the evolution of crystalline morphology was studied using a POM (Olympus BX51, Japan) fitted with an automated hot stage (Linkam THMS600). Blend films were sandwiched between a microscope slide and a coverglass. A charge-coupled device (CCD) camera (ProgRes C3, Germany) mounted on the microscope allowed the recording of the evolution of morphology as a function of temperature. The blend samples were heated above the melting temperature of PVDF (200 °C) to ensure complete miscibility and were kept isothermally at 200 °C for half an hour. After that, samples were cooled at a rate of 2 °C/min, up to the expected temperature of crystallization. At the crystallization temperature, samples were kept isothermally for 60 min to capture the evolving crystalline morphology.

Dielectric measurements were performed on compression molded disks of 10 mm diameter and 1.5 mm thickness using an Alpha-N Analyzer, Novocontrol (Germany) in a broad frequency range of $10^{-2} < \omega < 10^{7}$ Hz and in the temperatures range of 200 °C −120 °C with a step change of 5 °C. For the spectroscopy measurements at higher temperature (above the melting temperature of the blends) the samples were placed between two brass plates, separated by an annular Teflon spacer to maintain the sample geometry in the melt state. The same spacer was used for all the measurements in order to avoid errors due to differences in sample dimensions. The dielectric loss spectra were fitted using Havriliak−Negami (HN) empirical equations.

Phase morphologies and the localization of MWNTs in the annealed and quenched samples were evaluated using SEM at room temperature.

RESULTS AND DISCUSSION

Calorimetric Transition Temperatures. The blend samples are rendered amorphous by heating to 220 °C at a rate of 10 K/min and holding for a few minutes isothermally followed by rapid quenching to liquid nitrogen conditions. In the second heating cycle, the blends are heated at 10 K/min and slowly cooled to room temperature at 2 K/min to monitor the crystallization process in PVDF. DSC thermograms of PVDF/PMMA blends with or without MWNTs, in heating and cooling cycles, are shown in Figure 3a,b, respectively, and listed in Table 1. All the blends investigated here showed a single T_g, confirming the miscibility in the blends. It has been reported that in PMMA/PVDF blends, at concentrations of PVDF < 50 wt %, the T_g of the blends levels off at 40−50 °C as crystallization of the PVDF phase is completely suppressed.[7]

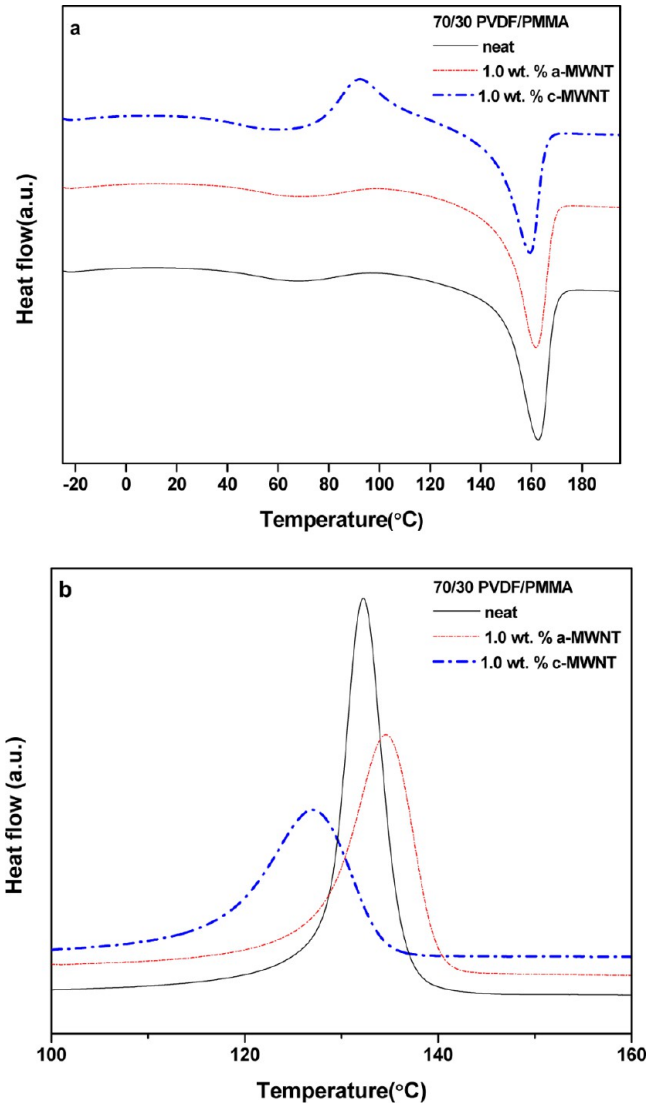

Figure 3. Melting (a) and crystallization thermograms (b) of 70/30 PVDF/PMMA blends with or without MWNTs.

Table 1. Calorimetric and Rheologically Determined Crystallization Induced Phase Separation Temperatures of Various Blends

composition	T_g (°C) (±1 °C)	T_m (°C)	T_c (°C)	T_{rheo} (°C) (±1 °C)
PVDF	−22	167	150	-
PMMA	110	-	-	-
PVDF/PMMA (70/30, wt/wt)	47	162	139	150
PVDF/PMMA (70/30) with 1 wt % a-MWNT	48	163	141	154
PVDF/PMMA (70/30) with 1 wt % c-MWNT	37	159	135	150

The T_g of the blends investigated here show a positive deviation from the linear relationship of Gordon−Taylor:

$$T_{g2} - T_{gB}(1 - \varnothing_1) + k(T_{g1} - T_{gB})\varnothing_1 = 0 \quad (1)$$

where T_{g1}, T_{g2}, and T_{gB} refer to the T_g's of PVDF, PMMA, and the blend, respectively. $\varnothing_1$ is the weight fraction of PVDF; k is $\Delta\alpha_{PVDF}/\Delta\alpha_{PMMA}$, and $\Delta\alpha$ is the difference between the thermal expansion coefficients. The width of the T_g depends on the magnitude of local composition fluctuations in the blends,

dx.doi.org/10.1021/jp4033723 | J. Phys. Chem. B 2013, 117, 8589−8602

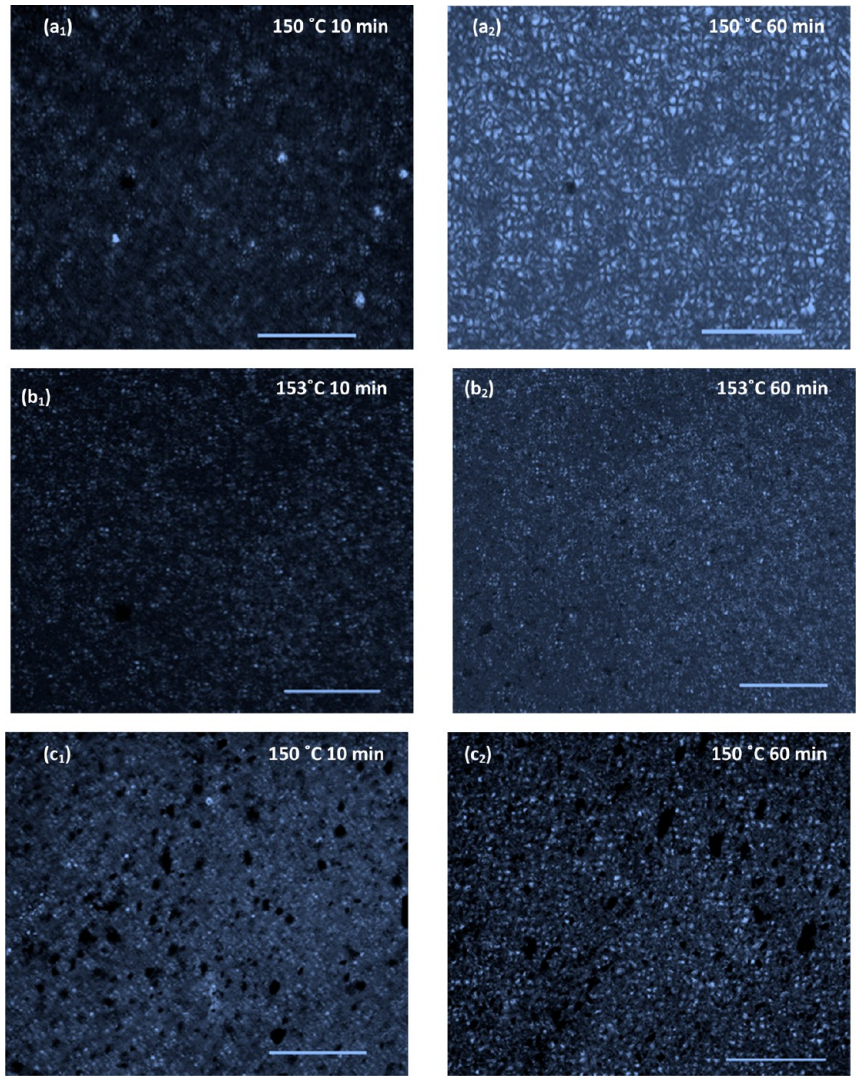

Figure 4. POM images for 70/30 PVDF/PMMA blends with and without MWNTs during isothermal annealing for the initial stages (a_1, b_1, c_1) and after 60 min of annealing (a_2, b_2, c_2). The upper row is for neat 70/30 PVDF/PMMA blends; the middle and the bottom rows are for 70/30 PVDF/PMMA blends with 1 wt % a-MWNTs and 1 wt % c-MWNTs, respectively (scale bar: 100 μm).

indicating their relative homogeneity or miscibility.[31] For partially miscible blends, the width of T_g can be as large as 30 °C (as in the case of the present system). Above the T_g, in some blends a small exotherm is observed around 60−80 °C, essentially suggesting that the quenched PVDF starts forming crystal nuclei, free from the restriction of the surrounding amorphous phases.[6] Blends with 1% a-MWNT show a slight increase in T_g and T_m, which might be due to the specific interactions like dipole−induced-dipole interaction between the $-NH_2$ functional moieties of a-MWNT and the $-CF_2$ group of PVDF between a-MWNTs and PVDF. Such interaction mimics physical cross-linking, thereby increasing the T_g. The T_c in the case of blends with a-MWNTs is also higher in contrast to both neat blends and blends with c-MWNTs. a-MWNTs enhances the crystal nucleation at relatively high temperatures and act as heteronucleating agents. Specific interaction between a-MWNTs and the PVDF matrix also favors the nucleating effect of MWNTs, which in turn augment T_c. As discussed earlier, dipoles induced by $-NH_2$ group of a-MWNTs further stimulate the conversion of α phase (*trans−gauche−trans−gauche′*) crystals into β (*trans−trans*) phase crystals in PVDF. Interestingly, the presence of c-MWNTs in the blends decreases both the T_g and the T_m. One plausible explanation could be that c-MWNTs act as diluents.[32] Furthermore, the blends with c-MWNTs also showed a reduced T_c. It is evident from DSC studies that the surface functional moieties on MWNTs, more specifically, the nature of interactions with PVDF, in turn govern the nucleation activity of MWNTs (see Table 1). It is well established that MWNTs act as heteronucleating agents, thereby promoting higher number of crystals; however, more interestingly, thicker and more stable lamellae have been observed in some cases wherein it is believed that the general orientation of the chains are parallel to the MWNT axis.

Crystalline Morphology: POM and SEM. The crystalline morphology of various PVDF/PMMA blends with and without MWNTs is studied using a POM. In order to probe the onset of crystallization in PVDF, melt miscible samples were slowly cooled to the calorimetric crystallization temperature (T_c), and the crystals were allowed to grow isothermally for 60 min. From optical images of neat 70/30 PVDF/PMMA blends (Figures 4a_1,a_2), we can clearly account for the development of spherulitic morphology of PVDF in this system. During isothermal annealing, initially small spherulites are developed,

dx.doi.org/10.1021/jp4033723 | J. Phys. Chem. B 2013, 117, 8589−8602

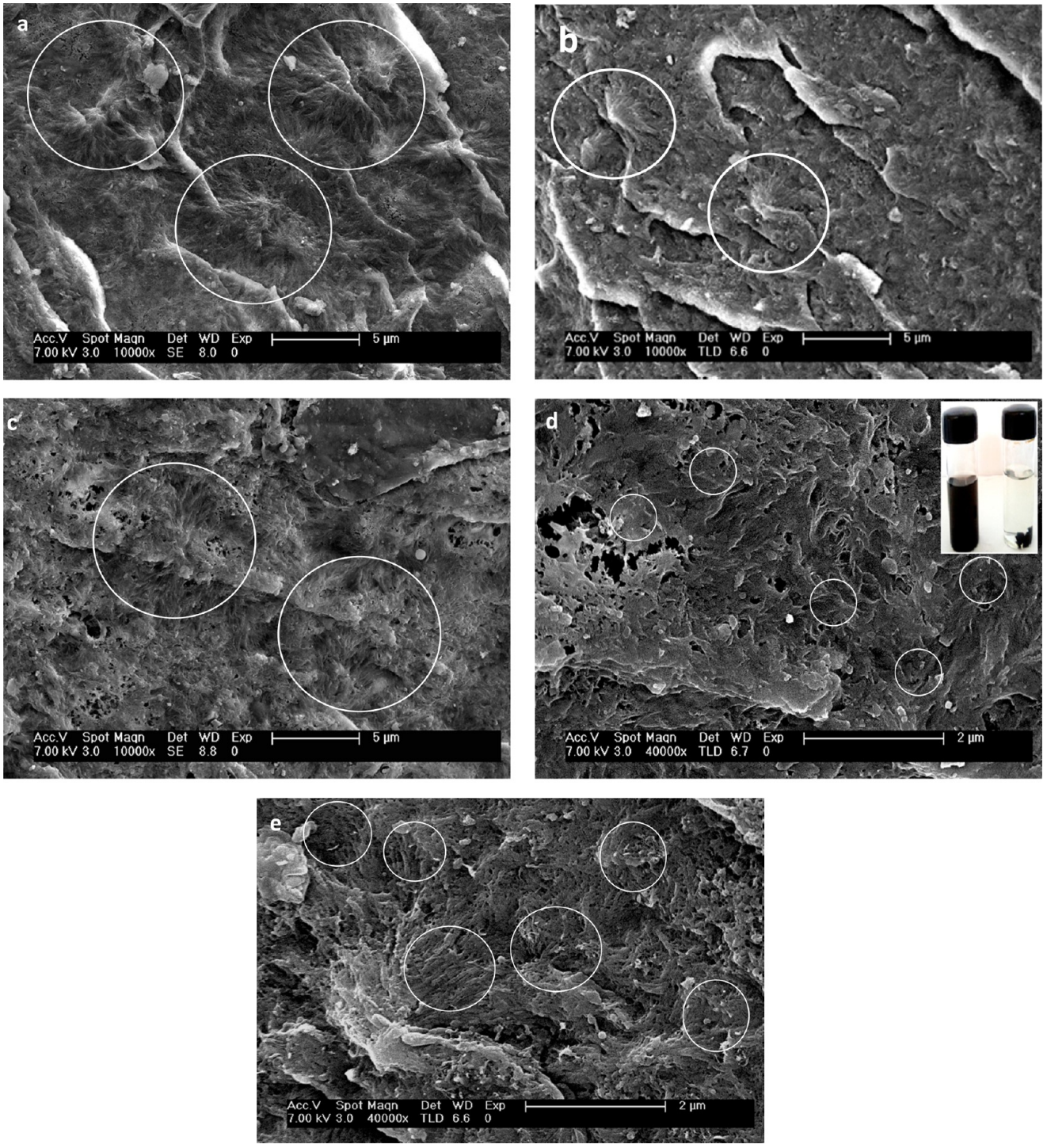

Figure 5. SEM micrographs of cryofractured and etched 70/30 PVDF/PMMA neat blends (a); blends with 1.0 wt % a-MWNT (b); blends with 1.0 wt % c-MWNT (c); high magnification images of blends with 1.0 wt % a-MWNT (d); and with 1.0 wt % c-MWNT (e). (The spherulites and the MWNTs appearing as white dots are indicated. Inset of panel d shows the selective localization of MWNTs in PVDF (left vial)).

which grew fully with time and attained a crystal−amorphous type of morphology. It is generally agreed upon that, during crystallization, the amorphous PMMA segregates in the interspherulitic regions of PVDF. We will discuss the segregation of the amorphous phases and the localization of MWNTs later on. It is clear from the optical images (Figure 4b_1,b_2 and c_1,c_2) that, with addition of MWNTs, the crystal size decreases to a reasonable extent. MWNTs act as nucleating sites, which increase the number of crystallizing nuclei; spherulites start impinging on each other, and this in turn decreases the size of the spherulites.[33] Specific interaction between the $-NH_2$ group of a-MWNTs and the $-CF_2$ group of PVDF, as inferred from FTIR, might provide better dispersion of MWNTs in the PVDF phase of the blends. This further promotes the crystal nucleation at relatively high temperatures, which is in close agreement with calorimetric crystallization temperatures (T_c). The large number of small sized crystals formed in 70/30 PVDF/PMMA blends in the presence of a-

dx.doi.org/10.1021/jp4033723 | J. Phys. Chem. B 2013, 117, 8589−8602

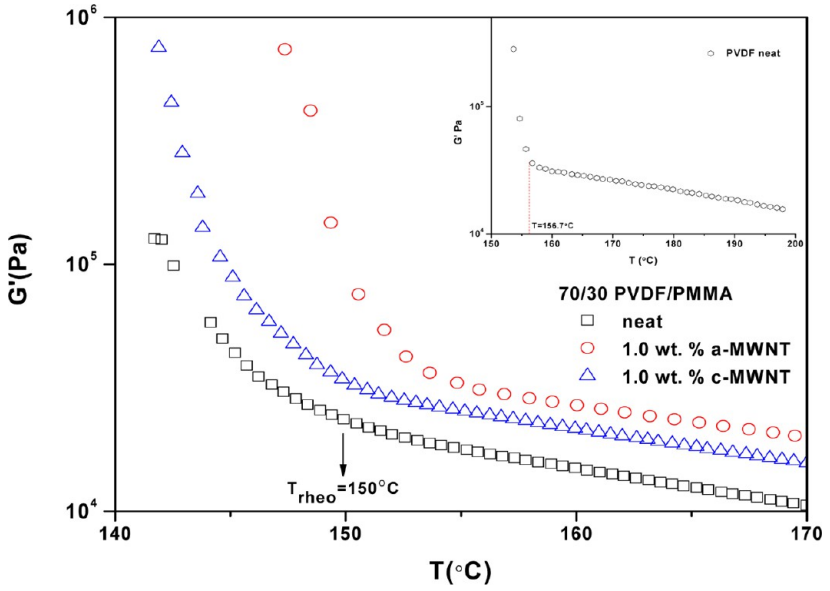

Figure 6. Dynamic temperature ramp (at 0.1 rad/s and 1% strain) for neat PVDF (inset) and 70/30 PVDF/PMMA blends with 1.0 wt % of MWNTs at a cooling rate of 0.5 °C/min.

MWNT (Figures 4b$_1$,b$_2$) are β-phase (*trans*−*trans*) crystals of PVDF. This is further supported by WXRD and FTIR. The phase transformation from α to β in the presence of a-MWNTs in PVDF is possibly due to the segmental flip-flop motion of PVDF chains, which is often associated with random orientation and improper spherulitic structure.[34] In the case of blends with c-MWNTs, the crystalline morphology consists of predominantly α-phase crystals.

The minimization of interfacial energy is the driving force for the particles to localize in a particular phase or at the interphase in binary blends. A quantitative estimation of wetting coefficient given by eq 2 gives an idea about the localization of MWNTs in blends provided the surface free energy (SFE) of the components, MWNTs, and the temperature dependency of SFE is known.

$$\omega_{12} = (\gamma_{p-B} - \gamma_{p-A})\gamma_{AB} \quad (2)$$

where, $\gamma_{p\text{-}B}$ and $\gamma_{p\text{-}B}$ are the interfacial tensions between MWNT and the constituents, and γ_{AB} is the interfacial tension between the constituents.[35] For $\omega_{12} > 1$, MWNTs would be located in PMMA, for $\omega_{12} < -1$, MWNTs would be located in PVDF, and for $-1 < \omega_{12} < 1$, MWNTs would be preferentially located at the interface. The interfacial tension between the constituents and between the constituents and the MWNTs are determined using the Owens−Wendt equation given by[36,37]

$$\gamma_{12} = \gamma_1 + \gamma_2 - 2\sqrt{\gamma_1^d \gamma_2^d} - 2\sqrt{\gamma_1^p \gamma_2^p} \quad (3)$$

The SFE of PMMA (41.1 mN/m at 25 °C) is higher than that of PVDF (25 mN/m at 25 °C), and, as per thermodynamic criterion, MWNTs would be localized in the PMMA phase of the blends.[38,39,37] This is also supported by the wetting coefficient calculations using eq 2. The melt viscosity of the PVDF phase is also much higher in comparison to that of PMMA ($M_{w,PVDF} \gg M_{w,\ PMMA}$). Interestingly, MWNTs are observed to be localized in the PVDF phase of the blends as observed form the solvent dissolution experiments and SEM (see next section). The specific interaction between MWNTs, and the PVDF matrix favors the localization of MWNTs in the PVDF phase. Such observations were reported earlier by Sumita et al. in PVDF/PMMA blends.[40] The presence of MWNTs in the PVDF phase has also altered the crystalline morphology and the calorimetric transition temperatures as inferred from POM and DSC analysis as a result of specific interactions.

Cryofractured and selectively etched (using glacial acetic acid to remove the PMMA phase) samples are investigated under SEM to confirm the localization of MWNTs in the blends. SEM micrographs of 70/30 PVDF/PMMA neat blends are shown in Figure 5a. PVDF spherulites are apparent from this micrograph (as indicated) and more interestingly, the pores in the interspherulitic regions are also very evident, which is a manifestation of the etched PMMA phase. As mentioned earlier, amorphous PMMA can segregate in the liquid-like interlamellar regions within the spherulites and in the interspherulitic regions. It is worth mentioning that previous reports suggest that PMMA is excluded from the crystalline−amorphous interphase of PVDF and segregates mainly in the interlamellar regions of PVDF, especially in blends with PVDF content >50 wt %. Figure 5b,c shows the SEM micrographs of 70/30 PVDF/PMMA blends with 1 wt % a-MWNT and 1.0 wt % c-MWNT, respectively. The overall crystalline-morphology remains by and large the same upon addition of MWNTs; however, the size and distribution of the spherulites are observed to be quite different in the case of MWNTs (as also inferred from POM). The high-resolution SEM images of the blends with MWNTs are shown in Figure 5d,e. MWNTs appear as white dots (as indicated) and are observed in the interspherulitic regions. This does not exclude the possibility of MWNTs in the liquid-like interlamellar regions of amorphous PVDF/PMMA miscibility. It has been reported earlier that, in the case of PA66/MWNT composites, the spherulites were observed to engulf the MWNTs resulting in a "globular" morphology consisting of nano hybrid "shish-kebab" structures.[41] It is noteworthy that during selective etching of PMMA from the blends, we did not observe any MWNTs in the solution, which further suggests that MWNTs are mostly localized in the amorphous phases of PVDF and/or in the

dx.doi.org/10.1021/jp4033723 | J. Phys. Chem. B 2013, 117, 8589−8602

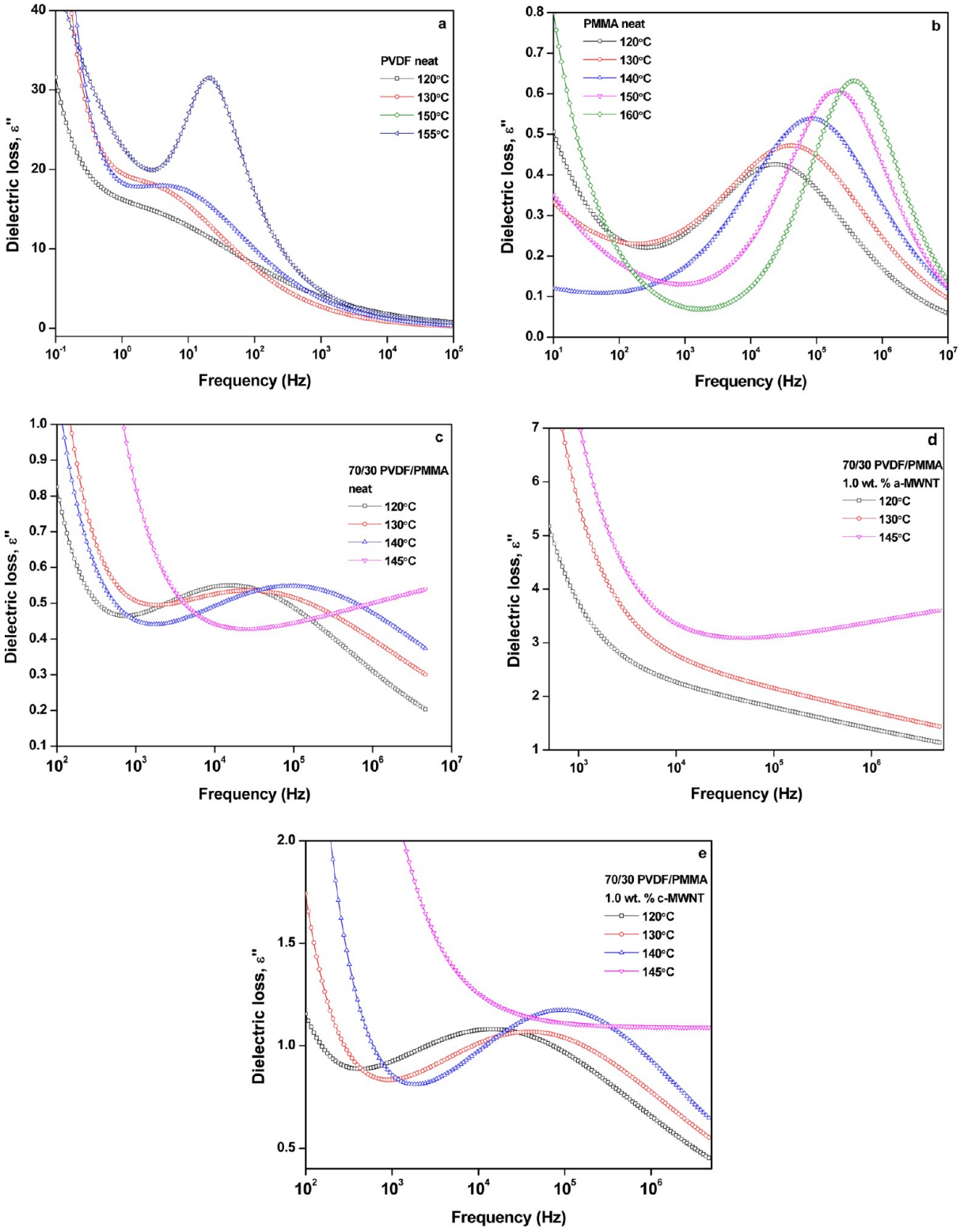

Figure 7. Dielectric loss as a function of frequency with temperature as a parameter for neat PVDF (a), neat PMMA (b), 70/30 PVDF/PMMA blends (c), blends with 1.0 wt % a-MWNT (d), and blend with 1 wt % c-MWNT (e).

interlamellar regions of PVDF/PMMA. Solvent-dissolution experiments further shed light on the preferential localization of MWNTs in the PVDF/PMMA blends (see inset of Figure 5d). Blend samples with 1 wt % MWNTs were annealed for 3 h at the calorimetric crystallization temperature (T_c) and quenched rapidly to arrest the phase morphology. Annealed and quenched samples were dissolved in the respective solvents (glacial acetic acid for PMMA and acetone for PVDF) and sonicated for 15 min. Although acetone is a common solvent for both the polymers, the dissolution kinetics are different. PVDF dissolves much more quickly than PMMA. It is observed that the blend solution in acetone appeared black in color

dx.doi.org/10.1021/jp4033723 | J. Phys. Chem. B 2013, 117, 8589−8602

immediately after dissolving, suggesting suspended MWNTs in the solution. This observation further manifests the strong affinity of MWNTs toward the PVDF phase of the blends.

Crystallization-Induced Phase Separation by Shear Rheology. Isochronal dynamic temperature ramps are performed to investigate the phase transition temperatures, induced by crystallization of PVDF phase, in PVDF/PMMA blends in the presence of MWNTs. The blend samples are rendered amorphous by holding at 200 °C for 30 min followed by cooling the melt at 0.5 °C/min to the phase-separated regime. During these tests, the axial force is compensated to take into account the volumetric changes occurring due to crystallization. Figure 6 shows the temperature dependence of G' for blends of PVDF/PMMA in the linear viscoelastic regime at a low frequency of 0.1 rad/s and at a cooling rate of 0.5 °C/min. The G' vs T for the neat PVDF is shown as an inset. As the stresses during the microstructural origin are of elastic in nature, we are interested only in the variation of G' as a function of temperature. G' appears to be linearly increasing with decreasing temperature. An abrupt increase in the G' at about 156 °C is observed and can be attributed with the crystallization process of PVDF (shown in Figure 6 inset) and is assigned as T_{rheo}. It is interesting to note that the calorimetric crystallization temperature (T_c) and the T_{rheo} differ by few °C as the signals are picked up from structures of different length scales. It is very evident from the literature that crystallization of PVDF leads to phase separation in PVDF/PMMA blend.[6,42] Cooling from a homogeneous melt to a temperature below the calorimetric melting point (T_m) results in crystallization of PVDF and the segregated amorphous portion forms a complex morphology. It is generally agreed upon that PMMA is excluded from the crystalline−amorphous interphase of PVDF, which is on the order of few nanometers and gradually replaces the liquid-like interlamellar PVDF region by PVDF/PMMA miscible phases.[43] As seen from Figure 6, neat PVDF/PMMA (70/30, wt/wt) blends show a slope change in G' vs T at ∼150 °C. With addition of 1 wt % a-MWNT, the T_{rheo} shifts to 154 °C, whereas in blends with c-MWNTs the T_{rheo} shifts to lower temperature. As discussed earlier, a-MWNTs facilitate heterogeneous nucleation, thereby up shifting the crystallization temperature of PVDF. This further augmented the phase separation in the blends. By contrast, c-MWNTs are found to decrease the calorimetric crystallization temperature in the blends; however, no appreciable change in T_{rheo} is observed. It is believed that both crystallization and liquid−liquid phase separation in PVDF/PMMA blends compete with each other; however, some studies also suggest that liquid−liquid phase separation precedes the crystallization-induced phase separation process.[5,44] While it is still debatable, a higher phase transition temperature determined rheologically (T_{rheo}) in contrast to calorimetric transitions cannot be assigned to liquid−liquid phase separation preceding crystallization-induced phase separation, as a similar break in slope in G' is also observed for the neat PVDF. Hence, we assign T_{rheo} to crystallization induced phase separation in PVDF/PMMA blends.

From the above results, there are several pieces of important information that can be deduced from a closer inspection. It is evident that surface functional groups on MWNTs has a strong influence on the overall crystalline morphology and the phase transition temperature as inferred from DSC, POM, and rheology. The presence of MWNTs in the PVDF phase, more specifically in the amorphous portions of the interspherulitic regions, can have strong influence on the various relaxations, which are governed by the cooperative segmental motion of the chains and show a strong dependency of temperature. Moreover, as the M_w of the constituents are sufficiently higher than the entanglement threshold (typically $\gg M_e$), the miscibility in the interzonal liquid-like amorphous regions can promote entanglement. Thus, the relaxation dynamics can be altered in the presence of MWNTs, as the length scales of the amorphous regions are reliant on the evolving crystalline phases, and is elaborated on in the next section.

Relaxations by Dielectric Spectroscopy. Broadband dielectric spectroscopy studies were conducted to probe the dielectric relaxations in the blends in presence of MWNTs. Figure 7a−e shows the dielectric permittivity (ε'') as a function of frequency at different temperatures for the neat constituents and for the blends of PVDF/PMMA (70/30, wt/wt) with and without MWNTs. Three types of relaxations have been identified in the case of PVDF: relaxations of the amorphous segments (α_a); relaxations associated with the crystalline regions (α_c), the origin of which has been identified as various forms of imperfections developed within the chains during crystallization and discontinuities within the interior of crystals;[8,16,45,46] and β relaxations corresponding to localized motions and often observed at low temperatures. The samples are cooled from the melt, and the spectra are captured at different temperatures and plotted as a function of frequency. Dielectric loss as a function of frequency at different temperatures for neat PVDF has been illustrated in Figure 7a. Relaxations corresponding to the amorphous segments of PVDF (α_a) could not be captured in the measured frequency window, and only the α_c relaxations could be mapped out. It is evident from Figure 7a that α_c diffuses and shifts to lower frequency with decreasing temperature. A sudden increase in ε'' is a result of high interfacial polarization, which is due to enhanced dc conductivity at low frequencies (<10 Hz). Moreover, at high temperatures, the migration of polar charges at low frequencies results in high polarization. The loss spectra has been fitted using the Haviriliak−Negami (HN) empirical equation.[47] The HN fit also considers DC conductivity contribution and is given as

$$\varepsilon^* = \varepsilon' - i\varepsilon'' = -i(\sigma_{dc}/\varepsilon_0\omega)^N + (\Delta\varepsilon/(1 + (i\omega_{\tau HN})^\alpha)^\beta) \quad (4)$$

where ε^* is the complex dielectric permittivity, σ_{dc} is the dc conductivity, ω is angular frequency ($\omega = 2\pi f$), $\Delta\varepsilon$ is the relaxation strength, and α and β are the fitting parameters ($0 \leq \alpha, \beta \leq 1$) describing symmetry and asymmetry broadening parameters, respectively, listed in Table 2. From the fitting parameters, dielectric strength $\Delta\varepsilon$ and mean relaxation time τ_{HN} were obtained. Dielectric relaxations for the neat PMMA as a function of frequency at different temperatures are shown in Figure 7b. At temperatures at or above the T_g, both the α and the β (which is due to localized motion of side groups < T_g) relaxations merge and form a single $\alpha\beta$ relaxation.[8] As expected the ε'' peak shifts to lower frequency as the temperature decreases from 160 to 120 °C. This is also accompanied by broadening of curve and also decreases in the peak intensity. As in the case of PVDF, the low frequency behavior (∼100 Hz) shows a strong effect of dipoles and migration of dipoles at higher temperature.

In crystalline blends of PVDF/PMMA, five types of relaxations are generally observed: α_a relaxation related with local segmental motions of amorphous phase of PVDF and is composition independent;[8] α_c relaxation associated with the

dx.doi.org/10.1021/jp4033723 | J. Phys. Chem. B 2013, 117, 8589−8602

Table 2. H−N Fitting Parameters for Various Blends

	temp. (°C)	τ (s)	$\Delta\varepsilon$	α	β
PVDF	120	9.24×10^{-2}	93.0	0.38	1.0
	130	3.12×10^{-2}	94.2	0.44	1.0
	140	1.30×10^{-2}	93.3	0.45	1.0
	145	4.80×10^{-3}	77.0	0.52	1.0
	150	3.52×10^{-3}	75.9	0.53	1.0
	155	1.73×10^{-3}	64.0	0.94	0.611
PMMA	120	6.06×10^{-6}	1.89	0.52	1.0
	130	3.37×10^{-6}	2.03	0.51	1.0
	140	1.80×10^{-6}	2.20	0.55	1.0
	150	7.53×10^{-7}	2.00	0.68	1.0
	160	4.25×10^{-7}	1.89	0.75	1.0
PVDF/PMMA 70/30	120	9.24×10^{-7}	3.62	0.37	1.0
	130	5.03×10^{-6}	4.29	0.31	1.0
	140	8.93×10^{-7}	3.60	0.37	1.0
	145	1.30×10^{-9}	11.8	0.13	0.96
PVDF/PMMA 70/30 1 wt % a-MWNT	120	7.90×10^{-4}	32.7	0.18	0.95
	130	8.56×10^{-4}	42.1	0.16	1.0
	140	3.34×10^{-7}	20.3	0.38	0.99
	150	1.29×10^{-9}	70.5	0.16	1.0
PVDF/PMMA 70/30 1 wt % c-MWNT	120	1.04×10^{-5}	7.87	0.34	1.0
	130	3.89×10^{-6}	7.55	0.35	1.0
	140	1.65×10^{-6}	7.20	0.40	1.0
	145	1.00×10^{-9}	27.8	0.01	1.0

molecular relaxations due to imperfections in crystalline phases; α_m relaxation (unlike in neat PVDF) signifies the molecular motions in the miscible amorphous PVDF/PMMA phase; and β relaxations of both the polymers. At high temperatures, well above the T_g of the blend, β relaxation of PVDF disappears and the β relaxations of PMMA merge with the α relaxation leading to $\alpha\beta$ relaxation. So the relaxations that interests us are α_c and α_m relaxations of PVDF and $\alpha\beta$ relaxations of PMMA. In the blends studied here, the concentration of PMMA is >20%, and it is envisaged that at these concentrations both the α_c and the α_m relaxations merge to form a single broad peak and are often dielectrically indistinguishable. It is observed from Figure 7c that by blending PMMA with PVDF, the α_c relaxations of PVDF shift toward higher frequency due to increase in imperfection in the crystalline lamellae. HN fitting functions for this blend system are given in Table 3, which confirms that the values of α shape parameter are closer to PVDF than to PMMA, which further confirms that the relaxation is more of PVDF origin. The absence of relaxation peak at 145 °C in the blend also indicates that the peak is mainly due to crystallization of PVDF.

In 70/30 PVDF/PMMA with 1 wt % a-MWNT, the dielectric loss due to α_c completely disappears in the low temperatures, i.e., 120−135 °C (Figure 7d). It is well reported that this disappearance of crystalline relaxations is mainly due to the presence of β-phase (*trans*−*trans*) crystals of PVDF. The absence of dielectric loss peak from blends with 1 wt % a-MWNT supports the presence of β-phase of PVDF in the blends. The latter can be attributed to specific interaction with the PVDF and is also supported by FTIR and WXRD. Blends with 1 wt % c-MWNTs (Figure7e) show the dielectric loss behavior similar to the neat PVDF/PMMA blend. The mean relaxation time τ_{HN} and the relaxation strength $\Delta\varepsilon$ (using HN function) for blends are listed in Table 2. $\Delta\varepsilon$ is given by

$$\Delta\varepsilon = \varepsilon_{stat} - \varepsilon_{\infty} \quad (5)$$

where, ε_{stat} and ε_{∞} are permittivities at low and high frequencies, respectively, and are related to relaxation region and dipole moment under study. There is an evident increase in $\Delta\varepsilon$ with the addition of a-MWNTs with respect to neat blends and can be attributed to the interaction between a-MWNT and the PVDF matrix. This type of interaction induces high dipole moment. $\Delta\varepsilon$ of c-MWNT lies in between the neat blends and a-MWNT. Mean relaxation time, τ, decreases in the presence of MWNTs in contrast to neat blends and is observed to be more prominent in the blends with a-MWNTs. MWNTs interrupt the molecular relaxations of PVDF, which leads to delay and shifts the relaxations to lower frequency. In the case of a-MWNTs, selective localization as well as specific interaction with PVDF matrix resulted in significant shifts to lower frequency and, in turn, less τ. It is also interesting to note that the amplitude of the dielectric loss in the neat blends and blends with MWNTs are significantly less in contrast to neat PVDF. This is, from an industrial viewpoint, an interesting finding and can be very useful information in designing electronic materials for various applications.

In the blends with MWNTs, the dielectric permittivity becomes very high at low frequencies and often masks the relaxations due to interfacial polarization.[48] To overcome this problem, "electric modulus" formalism has been proposed. Electric modulus is another method of probing molecular relaxations in composites and is defined as the inverse of permittivity and given as

$$M' = \frac{1}{\varepsilon^*} = \frac{1}{\varepsilon' - j\varepsilon''} = \frac{\varepsilon'}{\varepsilon'^2 + \varepsilon''^2} + j\frac{\varepsilon''}{\varepsilon'^2 + \varepsilon''^2} = M' + jM'' \quad (6)$$

where M' and M'' are real and imaginary parts of the electric modulus, respectively, and ε' and ε'' are real and imaginary parts of the permittivity, respectively.

The electric modulus for neat PVDF and 70/30 PVDF/PMMA blends with and without MWNTs is illustrated in Figure 8a,b. M'' is plotted as a function of M' in the frequency domain at different temperatures and are typically known as Cole−Cole plots and offers an advantage over ε' and ε'' especially in cases where ε'' show a considerable increase at low frequency and high temperature.[49] This approach is most suitable for describing interfacial relaxations in composites with moderate heterogeneity and HN approach best describes for the systems with high heterogeneity. Interestingly, M'' versus M' follows HN for all temperatures. For the neat PVDF at high temperatures (160−170 °C, Figure 8a), the HN plot is a complete semicircle ceasing at origin. At comparatively low temperatures (120−150 °C), the formed semicircle does not reach the origin, but rather intersects the M' axis and also is accompanied by an extra arc. Deviation from the origin is an evidence of dielectric relaxation.[50] It is quite interesting that the presence of an extra arc at low frequency is evident only at or below the T_c of PVDF and possibly due to existence of relaxation of interfacial polarization after crystallization, which does not exist at high temperature. Comparative HN plot for blends with and without MWNTs are given in Figure 8b. At higher frequencies, after a certain temperature, an extra arc is evident. This extra arc corresponds to dynamic heterogeneity in the system and appears at or below the crystallization-induced phase separation temperature. The amplitude of this secondary arc is increasing with decreasing temperature, which shows increasing amount of heterogeneity. In the case of neat blends

dx.doi.org/10.1021/jp4033723 | J. Phys. Chem. B 2013, 117, 8589−8602

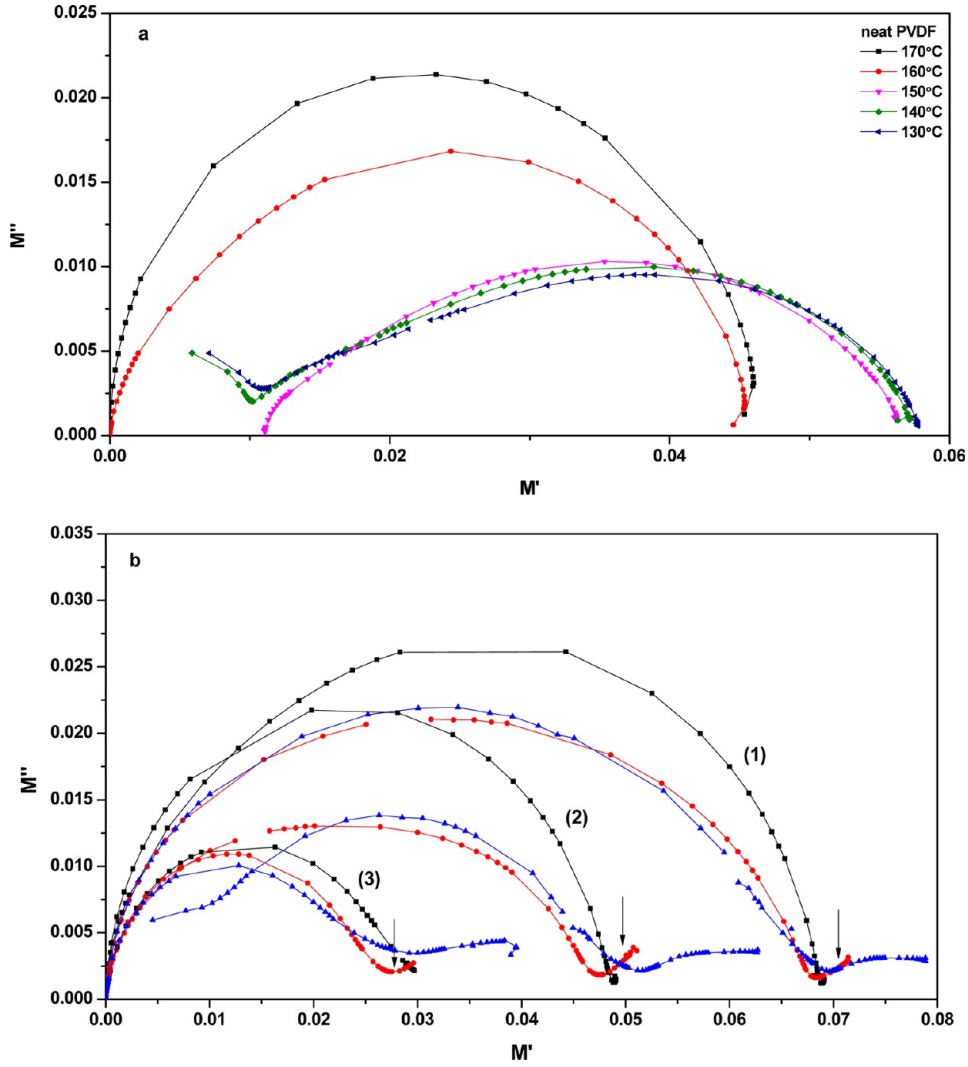

Figure 8. HN plots for neat PVDF (a) and for blends with and without MWNTs (b) (sub parts 1−3 in panel b indicate neat blends, blends with 1.0 wt % c-MWNT,s and blends with 1.0 wt % a-MWNTs, respectively, at different temperatures 170 °C (■), 145 °C (●), 135 °C (▲).

and blend with c-MWNTs, an extra arc appears at 145 °C (Figure 8b; regions 1 and 2). By contrast, for blends having a-MWNTs, this extra arc appears at 150 °C, manifesting in an early onset of dynamic heterogeneity with addition of a-MWNT (Figure 8b, region 3) in comparison to neat blends and the blend with c-MWNTs. These results are also in close harmony with POM, DSC, and rheology. The HN plot in Figure 8b also concludes that blends with a-MWNTs show a higher degree of heterogeneity and is also associated with high dielectric loss (also seen from ε'' vs ω plots) and moreover, the semicircle is completely formed as compared to neat blend and blends with c-MWNTs. This increasing heterogeneity shifts the whole relaxation process toward low frequency side, indicative of Maxwell−Wagner−Sillars (MWS)-type of relaxation in MWNTs. This is more evident in a-MWNTs.

Figure 9 shows the alternating current (AC) conductivity (σ_{AC}) behavior as a function of frequency at different temperatures for the neat blends and blends with MWNTs. The conductivity of the blends decays with decreasing temperature. In the neat blends (Figure 9a), the conductivity is observed to gradually decrease with temperature and become almost insulating at 140 °C (temperature below phase separation or below crystallization temperature of PVDF). The dipoles that were active at higher temperature and contributing to the bulk electrical conductivity cease with PVDF crystallization. By contrast, blend with 1% a-MWNT (Figure 9b) shows slightly higher conductivity as compared to neat blends at higher temperature. Even at lower temperatures (140 °C and below), blends with 1% a-MWNTs show a appreciable conductivity. Interestingly, in the blends with c-MWNTs, there is sudden drop in conductivity at or below the crystallization temperature of PVDF (see Figure 9c) and the absolute value of the conductivity is lower, especially below the crystallization temperature of PVDF. These phenomenal changes are possibly related with the crystalline morphology and more specifically with the ionic mobility in the crystalline−amorphous interface. From the conductivity data it is evident that the charge transport in the blends is of ionic nature. During crystallization, the probability of ion jumping decreases, and the charges rather accumulate at the crystalline−amorphous boundaries by the MWS phenomenon. The level of these interface charges is expected to increase with the size of the crystalline−amorphous interface as the mobility of the ions differs in the crystalline and in the amorphous regions. From the broadband dielectric spectroscopy, it is evident that blends with a-MWNTs showed a higher degree of heterogeneity and

dx.doi.org/10.1021/jp4033723 | J. Phys. Chem. B 2013, 117, 8589−8602

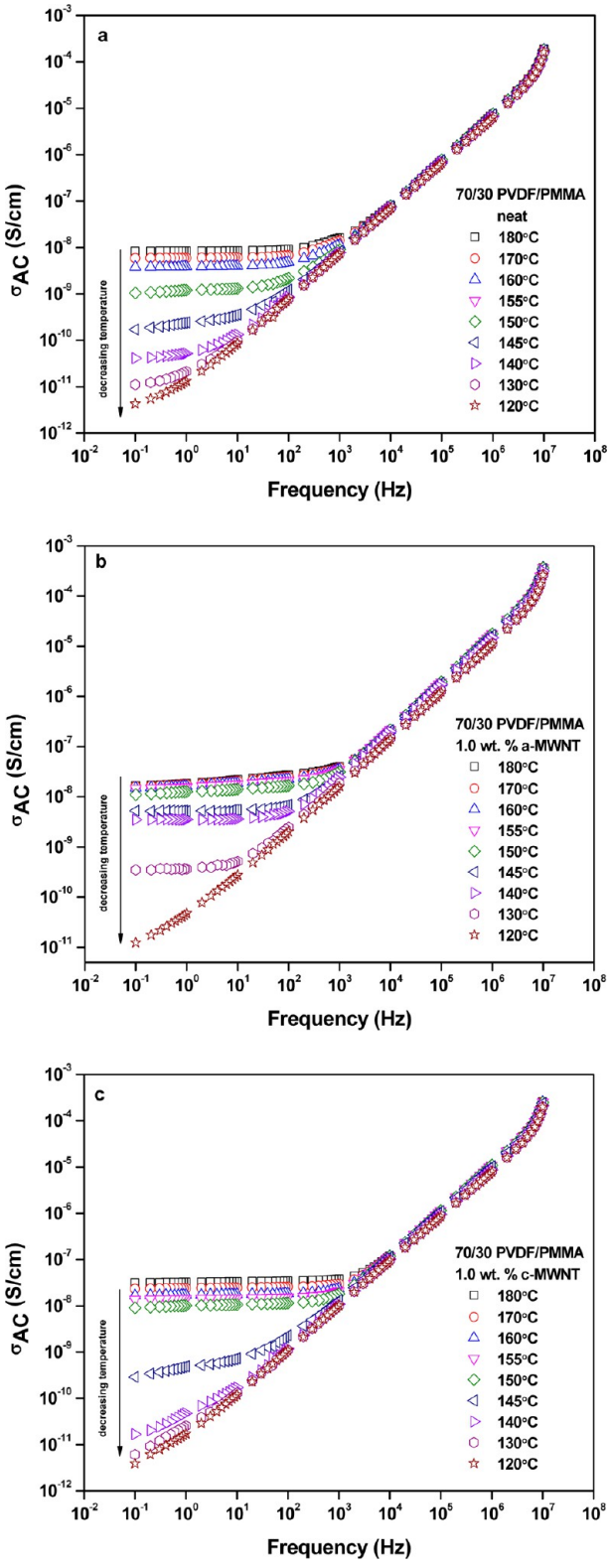

Figure 9. Frequency-dependent AC electrical conductivity (σ_{AC}) with temperature as a parameter for neat 70/30 PVDF/PMMA blends (a), blends with 1% a-MWNTs (b), and blends with 1% c-MWNTs (c).

hence, more charges are accumulated at the interface. This is also manifested in a higher degree of loses in the dielectric loss spectra. We can afford to say that the size of the crystalline−amorphous interphase in PVDF/PMMA blends, which is a direct consequence of the evolving crystalline morphology, dictates the overall dielectric behavior in the blends. The ionic mobility at these interfaces decreases and hence the conductivity decays with decreasing temperature. This, to some extent, was influenced by a-MWNTs, which aided in β-phase crystals in PVDF and has an orienting influence of dipoles and plausibly could be one of the reasons behind retaining the conductivity even below the crystallization of PVDF. The latter could also be due to cooperative motion of polymer chains in the interphase regions assisting in the charge transport.

CONCLUSIONS

To summarize, the effect of differently functionalized MWNTs (amine, ~NH_2 and acid, ~COOH) on the crystallization-induced phase separation and segmental relaxations was probed in situ by shear rheology and dielectric spectroscopy. Electron microscopy and selective etching confirmed the localization of MWNTs in the PVDF phase of the blends. Blends with only −NH_2-functionalized MWNTs (a-MWNTs) facilitated in heterogeneous nucleation in the blends and further augmented the rheologically determined crystallization-induced phase separation temperature in the blends. The a-MWNTs aided in the formation of β-phase (*trans*−*trans*) crystals in PVDF due to specific interactions (like dipole induced dipole interaction) between a-MWNTs and PVDF, as inferred from FTIR. The relaxations associated with the crystalline phase of PVDF (α_c) was completely absent in the blends with a-MWNTs, in contrast to neat blends and blends with c-MWNTs in the dielectric loss spectra. This was attributed to β-phase (*trans*−*trans*) crystals in PVDF in the presence of a-MWNTs. The dynamic heterogeneity, as seen from the HN fits, could be mapped by an extra relaxation at higher frequency in the blends and, moreover, the overall relaxations shifted to lower frequency in presence of MWNTs. The HN mean relaxation time (τ_{HN}) was observed to be delayed in the presence of MWNTs in the blends more prominently in a-MWNTs. The charge transport in the blends was directly related to the evolution of crystalline morphology and the crystal−amorphous interphase.

AUTHOR INFORMATION

Corresponding Author

*Phone: +91-80-22933407; Fax: +91-80-23600472; E-mail: sbose@materials.iisc.ernet.in.

Author Contributions

†Maya Sharma and Keshav Sharma contributed equally to this work.

Notes

The authors declare no competing financial interest.

ACKNOWLEDGMENTS

The authors gratefully acknowledge DAE-BRNS, India (DAEO0159), for the financial support, the spectroscopy and analytical test facility (SID), and the CeNSE characterization facility at IISc. The authors wishes to acknowledge discussions with Prof. Paula Moldenaers (KU Leuven) and Prof. Rajeev Ranjan (Materials Engineering, IISc) for extending the dielectric spectroscopy facility. We are also thankful to Arkema Inc. and Microplastics Pvt., Ltd. Bangalore, India, for providing us the polymer samples.

REFERENCES

(1) Nishi, T.; Wang, T. T. Melting-Point Depression and Kinetic Effects of Cooling on Crystallization in Poly(vinylidene fluoride) Poly(methyl methacrylate) Mixtures. *Macromolecules* **1975**, *8*, 909−915.

(2) Bernstein, R. E.; Cruz, C. A.; Paul, D. R.; Barlow, J. W. LCST Behavior in Polymer Blends. *Macromolecules* **1977**, *10*, 681−686.

(3) Saito, H.; Fujita, Y.; Inoue, I. Upper Critical Solution Temperature Behavior in Poly(vinylidene flouride)/Poly(methyl methacrylate) Blends. *Polymer* **1987**, *19*, 405−412.

(4) Greenall, M. J.; Buzza, D. M. A.; McLeish, T. C. B. Micelle Formation in Block Copolymer/Homopolymer Blends: Comparison of Self-Consistent Field Theory with Experiment and Scaling Theory. *Macromolecules* **2009**, *42*, 5873−5880.

(5) Tomura, H.; Saito, H.; Inoue, T. Light Scattering Analysis of Upper Critical Solution Temperature Behavior in a Poly(vinylidene fluoride)/Poly(methyl methacrylate) Blend. *Macromolecules* **1992**, *25*, 1611−1614.

(6) Ando, Y.; Yoon, D. Phase Separation in Quenched Noncrystalline Poly(vinylidene fluoride)/Poly(methyl methacrylate) Blends. *Polym. J.* **1992**, *24*, 1329−1336.

(7) Schneider, S.; Drujon, X.; Wittmann, J. C.; Lotz, B. Impact of Nucleating Agents of Pvdf on the Crystallization of PVDF/PMMA Blends. *Polymer* **2001**, *42*, 8799−8806.

(8) Mijovic, J.; Sy, J.-W.; Kwei, T. K. Reorientational Dynamics of Dipoles in Poly(vinylidene fluoride)/Poly(methyl methacrylate) (PVDF/PMMA) Blends by Dielectric Spectroscopy. *Macromolecules* **1997**, *30*, 3042−3050.

(9) Fang, Z.; Harrats, C.; Moussaif, N.; Groeninckx, G. Location of a Nanoclay at the Interface in an Immiscible Poly(ε-caprolactone)/Poly(ethylene oxide) Blend and Its Effect on the Compatibility of the Components. *J. Appl. Polym. Sci.* **2007**, *106*, 3125−3135.

(10) El-Mabrouk, K.; Belaiche, M.; Bousmina, M. Phase Separation in PS/PVME Thin and Thick Films. *J. Colloid Interface Sci.* **2007**, *306*, 354−367.

(11) Polios, I. S.; Soliman, M.; Lee, C.; Gido, S. P.; Rohr, S. K.; Winter, H. H. Late Stages of Phase Separation in a Binary Polymer Blend Studied by Rheology, Optical and Electron Microscopy, and Solid State NMR. *Macromolecules* **1997**, *30*, 4470−4480.

(12) Snyder, H. L.; Meakin, P.; Reich, S. Dynamical Aspects of Phase Separation in Polymer Blends. *Macromolecules* **1983**, *16*, 757−762.

(13) Utracki, L. A. *Polymer Blends Handbook*; Kluwer Academic Publishers: Dordrecht, The Netherlands, 2002; Vol. *1*.

(14) Vleminckx, G.; Bose, S.; Jan Leys, J.; Vermant, J.; Wübbenhorst, M.; Macosko, C.; Moldenaers, P. Effect of Thermally Reduced Graphene Sheet on the Phase Behavior, Morphology and Electrical Conductivity in Poly[(α-methyl styrene)-*co*-(acrylonitrile)/Poly-(methyl-methacrylate) Blends. *ACS Appl. Mater. Interfaces* **2011**, *3*, 3172−3180.

(15) Kapnistos, M.; Hinrichs, A.; Vlassopoulos, D.; Anastasiadis, S. H.; Stammer, A.; Wolf, B. A. Rheology of a Lower Critical Solution Temperature Binary Polymer Blend in the Homogeneous, Phase-Separated, and Transitional Regimes. *Macromolecules* **1996**, *29*, 7155−7163.

(16) Lipatov, Y. S.; Nesterov, A. E.; Ignatova, T. D.; Nesterov, D. A. Effect of Polymer-Filler Surface Interactions on the Phase Separation in Polymer Blends. *Polymer* **2002**, *43*, 875−880.

(17) Ginzburg, V. V. Influence of Nanoparticles on Miscibility of Polymer Blends. A Simple Theory. *Macromolecules* **2005**, *38*, 2362−2367.

(18) Peng, G.; Qiu, F.; Ginzburg, V. V.; Jasnow, D.; Balazs, A. C. Forming Supramolecular Networks from Nanoscale Rods in Binary, Phase-Separating Mixtures. *Science* **2000**, *288*, 1802−1804.

(19) Bose, S.; Khare, R. A.; Moldenaers, P. Assessing the Strengths and Weaknesses of Various Types of Pre-Treatments of Carbon Nanotubes on the Properties of Polymer/Carbon Nanotubes Composites: A Critical Review. *Polymer* **2010**, *51*, 975−993.

(20) Jiang, M.-J.; Dang, Z.-M.; Xu, H.-P. Giant Dielectric Constant and Resistance-Pressure Sensitivity in Carbon Nanotubes/Rubber Nanocomposites with Low Percolation Threshold. *Appl. Phys. Lett.* **2007**, *90*, 042914−042913.

(21) Yuan, J.-K.; Yao, S.-H.; Dang, Z.-M.; Sylvestre, A.; Genestoux, M.; Bai, J. Giant Dielectric Permittivity Nanocomposites: Realizing True Potential of Pristine Carbon Nanotubes in Polyvinylidene Fluoride Matrix through an Enhanced Interfacial Interaction. *J. Phys. Chem. C* **2011**, *115*, 5515−5521.

(22) Wang, L.; Dang, Z.-M. Carbon Nanotube Composites with High Dielectric Constant at Low Percolation Threshold. *Appl. Phys. Lett.* **2005**, *87*, 042903.

(23) Levi, N.; Czerw, R.; Xing, S.; Iyer, P.; Carroll, D. L. Properties of Polyvinylidene difluoride−Carbon Nanotube Blends. *Nano Lett.* **2004**, *4*, 1267−1271.

(24) Hou, Y.; Wang, D.; Zhang, X.-M.; Zhao, H.; Zha, J.-W.; Dang, Z.-M. Positive Piezoresistive Behavior of Electrically Conductive Alkyl-Functionalized Graphene/Polydimethylsilicone Nanocomposites. *J. Mater. Chem. C* **2013**, *1*, 515−521.

(25) Bose, S.; Bhattacharyya, A. R.; Haussler, L.; Potschke, P. Influence of Multiwall Carbon Nanotubes on the Mechanical Properties and Unusual Crystallization Behavior in Melt-Mixed Co-continuous Blends of Polyamide6 and Acrylonitrile Butadiene Styrene. *Polym. Eng. Sci.* **2009**, *49*, 1533−1543.

(26) Bormashenko, Y.; Pogreb, R.; Stanevsky, O.; Bormashenko, E. Vibrational Spectrum of PVDF and Its Interpretation. *Polym. Test.* **2004**, *23*, 791−796.

(27) Morra, B. S.; Stein, R. S. Melting Studies of Poly(vinylidene fluoride) and Its Blends with Poly(methyl methacrylate). *J. Polym. Sci., Part B: Polym. Phys.* **1982**, *20*, 2243−2259.

(28) Dillon, D. R.; Tenneti, K. K.; Li, C. Y.; Ko, F. K.; Sics, I.; Hsiao, B. S. On the Structure and Morphology of Polyvinylidene Fluoride Nanoclay Nanocomposites. *Polymer* **2006**, *47*, 1678−1688.

(29) Pawde, S. M.; Deshmukh, K. Investigation of the Structural, Thermal, Mechanical, and Optical Properties of Poly(methyl methacrylate) and Poly(vinylidene fluoride) Blends. *J. Appl. Polym. Sci.* **2009**, *114*, 2169−2179.

(30) Shah, D.; Maiti, P.; Gunn, E.; Schmidt, D. F.; Jiang, D. D.; Batt, C. A.; Giannelis, E. P. Dramatic Enhancements in Toughness of Polyvinylidene Fluoride Nanocomposites via Nanoclay-Directed Crystal Structure and Morphology. *Adv. Mater.* **2004**, *16*, 1173−1177.

(31) Yang, X.; Kong, X.; Tan, S.; Li, G.; Ling, W.; Zhou, E. Spatially-Confined Crystallization of Poly(vinylidene fluoride). *Polym. Int.* **2000**, *49*, 1525−1528.

(32) Chen, D.; Wang, M.; Zhang, W.-D.; Liu, T. Preparation and Characterization of Poly(vinylidene fluoride) Nanocomposites Containing Multiwalled Carbon Nanotubes. *J. Appl. Polym. Sci.* **2009**, *113*, 644−650.

(33) Chen, D.; Wu, M.; Wang, W.; Liu, T. Crystallization Behavior of Poly(vinylidene fluoride) Nanocomposites Containing Multiwalled Carbon Nanotubes. *J. Macromol. Sci., Phys.* **2010**, *49*, 1069−1082.

(34) Takahashi, Y.; Matsubara, Y.; Tadokoro, H. Mechanisms for Crystal Phase Transformations by Heat Treatment and Molecular Motion in Poly(vinylidene fluoride). *Macromolecules* **1982**, *15*, 334−338.

(35) Fenouillot, F.; Cassagnau, P.; Majesté, J. C. Uneven Distribution of Nanoparticles in Immiscible Fluids: Morphology Development in Polymer Blends. *Polymer* **2009**, *50*, 1333−1350.

(36) Fowkes, F. M. Attractive Forces at Interfaces. *Ind. Eng. Chem. Res.* **1964**, *56*, 40−52.

(37) Owens, D. K.; Wendt, R. C. Estimation of the Surface Free Energy of Polymers. *J. Appl. Polym. Sci.* **1969**, *13*, 1741−1747.

(38) Wu, S. Surface and Interfacial Tensions of Polymer Melts. II. Poly(methyl methacrylate), Poly(*N*-butyl methacrylate), and Polystyrene. *J. Mater. Chem* **1970**, *74*, 632−638.

(39) Nuriel, S.; Liu, L.; Barber, A. H.; Wagner, H. D. Direct Measurement of Multiwall Nanotube Surface Tension. *Chem. Phys. Lett.* **2005**, *404*, 263−266.

(40) Sumita, M.; Sakata, K.; Asai, S.; Miyasaka, K.; Nakagawa, H. Dispersion of Fillers and the Electrical-Conductivity of Polymer Blends Filled with Carbon-Black. *Polym. Bull.* **1991**, *25*, 265−271.

(41) Li, L.; Li, C. Y.; Ni, C.; Rong, L.; Hsiao, B. Structure and Crystallization Behavior of Nylon 66/Multi-Walled Carbon Nanotube Nanocomposites at Low Carbon Nanotube Contents. *Polymer* **2007**, *48*, 3452−3460.
(42) Osaki, S.; Kotaka, T. Electrical Properties of Form III Poly(vinylidene fluoride). *Ferroelectrics* **1981**, *32*, 1−11.
(43) Lin, D.-J.; Lin, C.-L.; Guo, S.-Y. Network Nano-porous Poly(vinylidene fluoride-*co*-hexafluoropropene) Membranes by Nano-Gelation Assisted Phase Separation of Poly(vinylidene fluoride-*co*-hexafluoropropene)/Poly(methyl methacrylate) Blend Precursor in Toluene. *Macromolecules* **2012**, *45*, 8824−8832.
(44) Lee, J. S.; Prabu, A. A.; Kim, K. J. UCST-Type Phase Separation and Crystallization Behavior in Poly(vinylidene fluoride)/Poly(methyl methacrylate) Blends under an External Electric Field. *Macromolecules* **2009**, *42*, 5660−5669.
(45) Nakagawa, K.; Ishida, Y. Annealing Effects in Poly(vinylidene fluoride) as Revealed by Specific Volume Measurements, Differential Scanning Calorimetry, and Electron Microscopy. *J. Polym. Sci., Part A-2: Polym. Phys.* **1973**, *11*, 2153−2171.
(46) Karasawa, N.; Goddard, W. A. Dielectric Properties of Poly(vinylidene fluoride) from Molecular Dynamics Simulations. *Macromolecules* **1995**, *28*, 6765−6772.
(47) Havriliak, S.; Negami, S. A Complex Plane Representation of Dielectric and Mechanical Relaxation Processes in Some Polymers. *Polymer* **1967**, *8*, 161−210.
(48) Hedvig, P. T. *Dielectric Spectroscopy of Polymers*; Wiley: New York, 1977.
(49) Davidson, D. W.; Cole, R. H. Dielectric Relaxation in Glycerol, Propylene Glycol, and *n*-Propanol. *J. Chem. Phy.* **1951**, *19*, 1484−1490.
(50) Tsangaris, G. M.; Psarras, G. C.; Kouloumbi, N. Electric Modulus and Interfacial Polarization in Composite Polymeric Systems. *J. Mater. Sci.* **1998**, *33*, 2027−2037.